Nanoscale Advances

REVIEW

View Article Online
View Journal | View Issue

Cite this: *Nanoscale Adv.*, 2021, **3**, 2180

Microfluidic synthesis of quantum dots and their applications in bio-sensing and bio-imaging

Yu Cheng, Si Da Ling, Yuhao Geng, Yundong Wang* and Jianhong Xu *

Bio-sensing and bio-imaging of organisms or molecules can provide key information for the study of physiological processes or the diagnosis of diseases. Quantum dots (QDs) stand out to be promising optical detectors because of their excellent optical properties such as high brightness, stability, and multiplexing ability. Diverse approaches have been developed to generate QDs, while microfluidic technology is one promising path for their industrial production. In fact, microfluidic devices provide a controllable, rapid and effective route to produce high-quality QDs, while serving as an effective *in situ* platform to understand the synthetic mechanism or optimize reaction parameters for QD production. In this review, the recent research progress in microfluidic synthesis and bio-detection applications of QDs is discussed. The definitions of different QDs are first introduced, and the advances in microfluidic-based fabrication of quantum dots are summarized with a focus on perovskite QDs and carbon QDs. In addition, QD-based bio-sensing and bio-imaging technologies for organisms of different scales are described in detail. Finally, perspectives for future development of microfluidic synthesis and applications of QDs are presented.

Received 7th November 2020
Accepted 13th February 2021

DOI: 10.1039/d0na00933d

rsc.li/nanoscale-advances

1 Introduction

Quantum dots (QDs) have emerged as an innovative material that has attracted great attention in the fields of nanotechnology and nanoscale science. They are 5–20 nm sized nanoparticles whose excitons are confined in all three spatial dimensions. Different from macroscopic materials possessing continuous energy levels, QDs are characterized by their discrete energy levels, which lead to their excellent optical performance.[1] Through electron transfers between the valence band and the conduction band, QDs exhibit obvious photoluminescence (PL) characteristics. Both the intensity and wavelength of excited fluorescence (FL) are closely related to the size of QDs. In addition, QDs demonstrate high luminescence and quantum yield (QY), narrow and symmetrical photoluminescence, as well as excellent photostability. These superior optical characteristics make QDs an ideal alternative in biomedical applications that can replace traditional organic dyes or fluorescent probes like fluorescent proteins.[2,3] When functionalized with specific affinity ligands, QDs have been utilized as fluorescent labels for the detection of biomolecules or target imaging.[4–6] Among diverse types of QDs, the CdX (X =

The State Key Lab of Chemical Engineering, Department of Chemical Engineering, Tsinghua University, Beijing 100084, China. E-mail: xujianhong@tsinghua.edu.cn; wangyd@tsinghua.edu.cn

Yu Cheng received his bachelors degree in chemical engineering from Tsinghua University in 2019. Since 2019, he has been working as a masters candidate in the group of Prof. Jianhong Xu, in the Department of Chemical Engineering at Tsinghua University. His research interests include functional nanoparticle preparation and structure design for biological applications.

Si Da Ling received his bachelors degree in Chemical Engineering from McGill University in 2019. Since 2019, he has been working in the group of Prof. Jianhong Xu as a masters candidate, in the Department of Chemical Engineering at Tsinghua University. His research mainly focuses on the preparation of functional microparticles and microencapsulation of cells or cellular substances for biomedical applications.

S, Se, Te) group is the most studied, but the potential cytotoxicity of the heavy metal element limits its wider application in the field of biology. As a result, more cadmium-free QDs have been developed, among which perovskite QDs and carbon dots have particularly drawn great attention. After all, for all groups of QDs, the regulation of QDs' properties highly depends on precise control of the synthesis reaction conditions.

Microfluidic-based systems, with their accurate controllability under the reaction conditions, have attracted researchers' interest for the generation of nanomaterials. Previous studies on QDs were mostly carried out in batch reactors. Despite the relative simplicity, they suffered from uncontrollable reactions and difficulty in maintaining the reproducibility between different batches. Compared to traditional batch reactors, microfluidic-based microreactors exhibit accurate controllability under the reaction conditions, such as temperature, pressure, and concentration distribution.[7] Specifically, most bottom-up synthesis routes of QDs consist of two distinct phases: nucleation and growth. These two processes can be precisely modulated by adjusting the parameters of microreactors in order to generate QDs of desired size, morphology and composition. Furthermore, because of the high sealing performance of micro-reactors, inert gas protection, which is usually essential in the batch production, can be discarded in the microfluidic synthesis of many groups of QDs. These changes brought by microfluidics highly improved both the safety and efficiency of synthesis crafts. Moreover, the scope of attaching a programmed controller or online detector to microfluidic devices further enables high automation and *in situ* research of QDs.[8–10]

Preliminary progress has been made in microfluidic synthesis of QDs. The application of QDs in more complicated and valuable biological scenarios through microfluidic technologies has been reported and optimized. This review mainly focuses on the microfluidic synthesis and applications of different types of QDs, especially of the newly emerged carbon dots and perovskite QDs. First of all, we will introduce existing methods for producing QDs from microfluidics, with achievements in the last decade highlighted. Moreover, we will discuss the application of QDs in biosensing and bioimaging, especially for living species of different scales. Finally, current challenges and future perspectives in the microfluidic synthesis of QDs and their applications will be briefly discussed.

Prof. Jianhong Xu received his BSc and PhD at Tsinghua University in 2002 and 2007, respectively. He continued his research at Tsinghua University as a postdoctoral fellow after graduation. He finished the postdoctoral program in May 2009 and became a formal faculty of the Department of Chemical Engineering, Tsinghua University. He was a visiting scholar in Prof. David Weitz's lab at Harvard University from 2012 to 2013. Currently, his research areas are microstructured chemical systems, multiphase microfluidic technology, and functional material synthesis. He has more than 160 peer-reviewed publications. He was awarded the title "Lab on a Chip Emerging Investigator" in 2012. He got the "Excellent Young Scientists Fund" from the National Natural Science Foundation of China (NSFC) in 2013. In 2016, he was awarded the title Young Scholar of "Chang Jiang Scholars Program of China" of the MOE.

2 Microfluidic synthesis of quantum dots

2.1 Quantum dots

As early as 1983, Brus *et al.*[11] produced 4.5 nm CdS nanoparticles in aqueous solution. These nano-sized zero-dimensional materials showed obvious quantum size effect, exhibited photoluminescence, and finally led to the invention of the concept, *i.e.*, quantum dots. In the following 40 years, various synthesis approaches of different quantum dots were developed for application in different scenarios. While metal–nonmetal compound traditional semiconductor QDs have been well studied, new mono and trinary QDs began to draw attention. Owing to their high quantum efficiency and tunable emission wavelength, QDs have shown potential in bio-optical applications. Herein, pathways to fabricate QDs with different compositions have been developed. Compared to traditional semiconductor QDs, carbon dots and perovskite QDs are typical new quantum dots showing great potential in bio-sensing and bio-imaging.

2.1.1 Semiconductor quantum dots. As shown in Table 1, semiconductor QDs, usually consisting of metal and nonmetal elements, can be classified as II–VI group, III–V group, IV–VI group, I–III–VI group, IV group, *etc.* according to the groups to which the constituent elements belong. Fig. 1 shows that different types of QDs exhibit tunable photoluminescence and emission ranges.

As mentioned above, CdS QDs were first found to exhibit great optical and electrochemical properties, and led a research tide to CdX QDs in the following years. Murray *et al.*[12] produced high-quality monodisperse CdSe nanoparticles from organometallic reagents by carefully controlling their growth speed. Later research reported that the coordinating solvent could help to control the growth and stabilize the resulting colloidal dispersion, leading to safer methods of synthesizing CdX QDs.[13,14] Noticeably, Cd-containing QDs possess potential

Table 1 Summary of semiconductor QDs

Elemental composition	Typical QDs
II–VI	CdS, CdSe, CdTe, ZnO, ZnS, ZnSe, ZnTe
III–V	InP, InAs
IV–VI	PbS, PbSe, SnS, SnSe
I–III–VI	$CuInS_2$, $CuInSe_2$
IV	Si, Ge

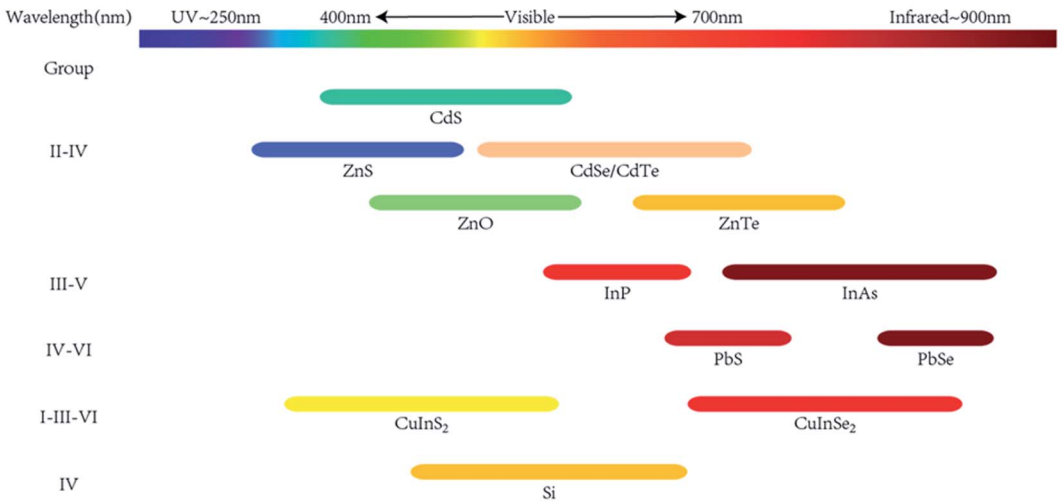

Fig. 1 Spectral range of emission for the most widely studied types of semiconductor NCs.

toxicity. Zinc, in the same group as cadmium but with lower cytotoxicity, was utilized to replace cadmium to form non-cadmium QDs. As a result, ZnO,[15] ZnS,[16] ZnSe and ZnTe[17] quantum dots have been previously reported by different research groups. On the other hand, the complex and mosaic surface on CdX QDs usually induces middle energy level. These structure declines luminescent transition between the band gap and conduction band, thereby lowering the stability and photoluminescence quantum yields. Core–shell structures can solve this problem. Dabbousi *et al.*[18] added diethylzinc and hexamethyldisilathiane to form a ZnS shell on CdSe QDs and produced CdSe@ZnS core–shell QDs, increasing the quantum yield from 5% to 50% when compared with single-core CdSe QDs. Furthermore, the ZnS shell would decrease the toxicity of the core QDs by preventing the release of Cd^{2+}, and promote its biological applications.

While II–VI group QDs show great fluorescence, the potential release of cadmium limits their *in vivo* application. On the other hand, III–V group QDs show outstanding potential because of their low toxicity. Especially, InP QDs can serve as a non-cadmium fluorescence label to replace CdSe QDs, and InAs QDs are also utilized in the near-infrared (NIR) emission area. Compared to II–VI group QDs, bonds in III–V QDs show more ionic character rather than covalent character, which demands harsher reaction conditions and more complicated precursors for their synthesis. Guzelian *et al.*[19] synthesized InP QDs by reacting $InCl_3$ and $P(SiMe_3)_3$ in a solution of TOPO, showing broader size dispersions (~20%) and lower quantum yield (1%) when compared to CdSe QDs. Similar to II–VI QDs, core–shell structures were formed to increase both quantum yield (QY) and stability. Thick ZnSeS shells with gradient composition were deposited onto InP cores and improved QY as high as 81% was achieved.[20] Alivisatos *et al.*[21] produced InAs QDs with $InCl_3$ and $As(SiMe_3)_3$ at 240–265 °C. Compared to InP QDs, InAs QDs possess a smaller band gap, enabling near-infrared emission (650–900 nm) with smaller particle size, where light absorption and scattering by hemoglobin and water are minimized.

IV group QDs are another fascinating material owing to their high stability and low toxicity. Crystal silicon is a common inorganic semiconductor material, and silicon turns into a direct band gap material with particle size decreasing to 5 nm. This change led to the short life of charge carriers, which is necessary for high PL efficiency. Luminescent silicon QDs were first produced by Werwa *et al.*[22] with the laser ablation technique in 1994. In this research, silicon QDs with a size of 2–3 nm were produced by focusing a laser on polycrystalline silicon, emitting ~650 nm peak light using a ~350 nm exciting laser beam. Due to the inorganic surface of silicon QDs, pure silicon QDs are insoluble in water, limiting their use in aqueous biospace. Kang *et al.*[23] converted H-terminated silicon QDs of 3 nm diameter into water-soluble uniform-sized silicon QDs with controlled oxidation in an $EtOH/H_2O_2$ solution. These silicon QDs are characterized with Si/SiO_xH_y core–shell nanostructures and can be fine-tuned to emit light in seven different colors from pink to blue, exhibiting excellent photocatalytic activity in the visible range. Silicon QDs proved to be less toxic at high concentrations in mitochondrial assays and lactate dehydrogenase (LDH) assays, which evidences their potential application for *in vivo* imaging.[24,25] More approaches to generate functional silicon QDs have been developed in the past 20 years,[3] and possible mechanisms of photoluminescence prove that the emission features strongly depend on the silicon nanostructures such as surface configurations.[26]

I–III–VI QDs are also known as ternary metal chalcogenide QDs, and are usually found in a normal combination as ABE_2 (A = Cu, Ag; B = In, Ga, Fe; E = S, Se). I–III–VI QDs could be derived from II–VI QDs by replacing two divalent metal cations with one monovalent and one trivalent cation. Such ternary QDs have drawn attention not only because of the absence of the toxic cadmium, but also owing to the tunable stoichiometry of the constituting elements. The latter property could help to regulate chemical and photoluminescence features of the generated QDs. Allen *et al.*[27] reported a series of $CuInSe_2$ QDs of varying stoichiometries that exhibit photoluminescence from

red to near-infrared. In this research, the choice of metal halides and growth temperatures was carefully made to control the size and composition of the resulting QDs. During the growth phase, $CuIn_5Se_8$ exhibited PL from 650 to 700 nm. Meanwhile, $CuIn_{2.3}Se_4$ showed PL from 900 to 975 nm, and their QY increased to 25%, which is higher than those of the historically reported I–III–VI QDs but still lower than those of II–VI semiconductor QDs. Furthermore, Li *et al.*[28] prepared $CuInS_2$ QDs in the non-coordinating solvent octadecene and overcoated the generated QDs on a ZnS shell. These QDs exhibited a luminescence range of 550–815 nm and maximum fluorescence quantum yield of 60%, which is the first report on the application of multinary Cu-based chalcogenide QDs in bioimaging.

2.1.2 Carbon quantum dots. Carbon QDs exhibiting photoluminescence were first found in the electrophoretic analysis of carbon nanotubes in 2004.[29] Carbon QDs do not consist of any metal elements and demonstrate good biocompatibility, low toxicity, and great biomedical application potential.[30] Thus it is often considered as a satisfactory functional material to replace traditional semiconductor QDs. Noticeably, although some researchers regard carbon dots (CDs) the same as carbon QDs,[31] they are not identical in concept. Many researchers categorize carbon dots into graphene quantum dots (GQDs), carbon quantum dots (multiple-graphene layered GQDs), carbon nanodots (CDs with an amorphous nature), and non-conjugated polymeric dots.[32–34] In this review, basic concepts of carbon dots are discussed with regard to fluorescent carbon-based nanoparticles.

The synthesis routes of CDs are divided into 2 types: top-down methods and bottom-up methods. Since CDs were first discovered during the electrochemical etching of carbon nanotubes, top-down methods have been developed to produce crystalized carbon QDs. Because of the high availability of bulk carbon material and low emission of toxic gases, electrochemical etching of carbon materials has been widely explored to fabricate CDs. Zhou *et al.*[35] produced blue luminescent CDs by applying circulating voltage on multiwalled carbon nanotubes (MWCNTs). Lu *et al.*[36] developed a one-pot electrochemistry method to prepare fluorescent carbon dots by the exfoliation of a graphite electrode, which allows upward scalability in terms of the production of bulk quantities of CDs. On the other hand, the bottom-up strategy has been used to develop flexible synthesis routes that allow a wide range of feasible precursors. These features have attracted more interest especially for their applications in the continuous and stable production of CDs. Bourlinos *et al.*[37] utilized ammonium carboxylate salt as the precursor, heated the salt in air at 300 °C, and produced modified photoluminescent CDs. Peng *et al.*[38] reported a simple aqueous solution route to prepare CDs from carboxylates, but these CDs showed a low quantum yield. The Zhu group[39] developed high quantum yield CDs with approximately 80% QY, which almost equals that of fluorescent dyes. CDs were produced by first condensing citric acid and ethylenediamine, whereupon they formed polymer-like CDs, and then carbonatizing them to produce QDs. In this system, the surface-state (molecule) emission plays a leading role in the high luminescence of the CDs, confirmed by a QY decrease when destructing the photochemical center *via* irradiation with high-power UV light. Microwave was also utilized to accelerate the processes of condensation and carbonation, achieving rapid synthesis of high-quality CDs.[40]

Furthermore, in the bottom-up strategy, alternative precursor molecules allowed greener and environment-friendly synthesis routes of CDs. Wang *et al.*[41] developed a one-step approach to fabricate CDs, where sustainable vegetables like spinach were utilized as the carbon source and deionized water as the solvent. The Guo group[42] reported the sustainable fabrication of highly fluorescent CDs (QY $\sim$ 45%) from food waste and turtle shells, and demonstrated their successful applications in anti-counterfeiting. Besides realizing green synthesis routes, the design of specific precursors could help to modulate the resulting carbon dots to achieve specific functions *in situ*. Chandra *et al.*[43] mixed amikacin, a synthetic amino glycoside antibiotic, with di-ammonium hydrogen citrate, kept them at 300 °C, and produced CDs. In this research, amikacin was conjugated with fluorescent CDs for selective *E. coli* detection, exhibiting a quantum yield of 12.35% at an excitation wavelength of 340 nm and proving to be able to detect the bacterial cell of *E. coli* with a low detection limit of 552 cfu mL^{-1}.

2.1.3 Perovskite QDs. The term 'perovskite' refers to a category of materials that share the same structure form as the mineral $CaTiO_3$. Perovskite material has the general formula ABX_3, where A represents the relatively bigger monovalent cation, B represents the divalent metal cation, and X stands for the halide anion (Cl, Br, I). Specifically, B-site cations are in an octahedral coordination with six X-site ions, and A-site cations should fit the BX_6 octahedral cavity. An unsatisfactory radius ratio could result in the deformation of the octahedron and affect the properties of the material. This structural framework provides opportunities to tune the composition and performance of QDs.

Perovskite QDs are mainly classified into two distinct types, hybrid organic–inorganic perovskites (HOIPs) and all-inorganic perovskites (AIPs). The first known HOIP QDs, $MAPbX_3$ (MA = methylammonium; X = Cl, Br or I), were reported in 1978[44] and then this type of perovskite QDs were developed as optoelectronic materials in the following years.[45,46] Unfortunately, HOIP QDs suffer from poor stability in air (oxygen and moisture), under heat and under ultraviolet light.[47] Compared to HOIP QDs, in AIP QDs, cesium replaces the organic cation, which brings higher stability, thereby extending their application range. Protesescu *et al.*[48] reported a hot-injection synthesis method of monodisperse $CsPbX_3$ (X = Cl, Br or I) QDs with bright (QY = 50–90%), stable and widely tunable photofluorescence. In this work, the fluorescence spectra of $CsPbX_3$ QDs could be tuned by controlling the ratio of halides and particle size. While hot-injection stands out to be the most successful and most delicate method to obtain the highest quality of perovskite QDs, some room-temperature methods have been recently developed. Li *et al.*[49] reported a ligand-assisted reprecipitation (LARP) method to produce high-QY perovskite QDs. The LARP reaction can be realized by pouring two precursor solutions into a vessel to induce supersaturated

precipitation at room temperature but it could still produce perovskite QDs at a QY of 80%.

One challenge in the application of perovskite QDs in the biomedical field is the potential toxicity of lead. Less toxic tin was used to replace Pb in $CsPbX_3$ QDs. Jellicoe *et al.*[50] produced $CsSnX_3$ perovskite QDs by the hot-injection method but obtained a rather low quantum yield at 0.14%. On the other hand, Zhang *et al.*[51] chose to utilize the heterovalent substitution of divalent lead (Pb^{2+}) with trivalent antimony (Sb^{3+}) to produce brightly luminescent $Cs_3Sb_2Br_9$ QDs, whose quantum yield was as high as 46%. Another challenge is to enhance the stability of perovskite QDs. One simple and effective method is to build surface coating. Zhou *et al.*[52] synthesized perovskite QDs in a PVDF membrane, and these QDs maintained high PL efficiency in water and UV light. MOF frameworks were also utilized to solve the problem of stability. Zhang *et al.*[53] reported an approach to realize luminescent perovskite NCs inlaid in Pb-based MOFs. In this case, perovskite QDs were kept stable in MOFs, and the luminescence was quenched with polar solvent impregnation that destroys the MOF matrix.

2.2 Reactors for microfluidic synthesis of QDs

Microfluidic technology offers the handle to manipulate microfluids at miniature volume from nanoliters to microliters within systems of microchannels whose dimensions range from tens to hundreds of micrometers. This technology has attracted increasing attention in recent years because of its outstanding heat and mass transfer efficiency. The efficiency of transfer originates from the large area-to-volume ratio and short diffusion distance in micro-devices. Therefore, a stable and desirable environment for the preparation of QDs can be easily achieved in microreactors. As shown in Fig. 2,[54] according to the flow pattern of the liquid in a microchannel reactor, microreactors can be divided into three types: continuous laminar flow microreactors, segmented flow microreactors, and droplet-based microreactors.

Continuous laminar flow microreactors are suitable for single phase liquid flows and have developed as the most widely used strategy to produce QDs. Continuous laminar flow microreactors are characterized by their convenient availability

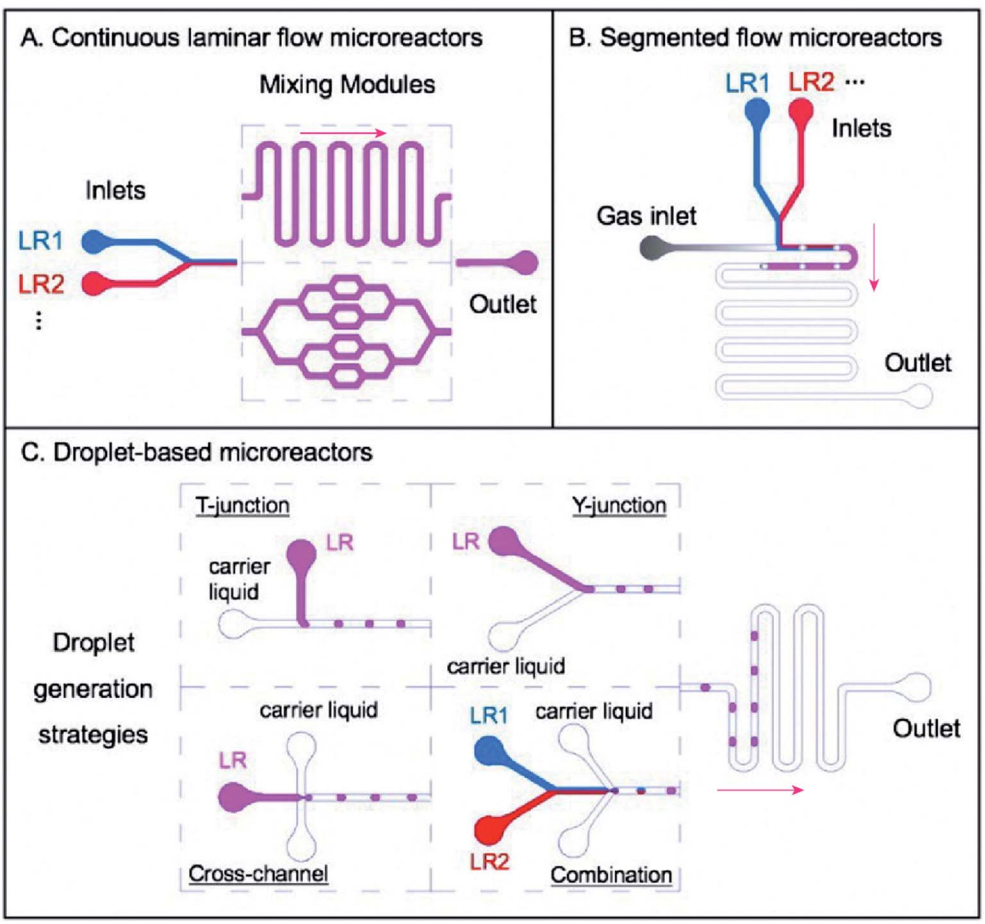

Fig. 2 Three main categories of microreactors: (A) continuous laminar flow microreactors, in which single phase flows of different liquid reagents (LR1, LR2…) are introduced into the systems, going through subsequent mixing modules such as winding microchannels and distributive mixing based mixers; (B) segmented flow microreactors, which usually consist of several liquid phase flows for introducing certain reagents (LR1, LR2…) and one gas phase flow to create 'bubbles' for separating segments of reagents; and (C) droplet-based microreactors, with which different strategies for droplet generation could be developed, including T-junction, Y-junction, cross-channel, and a combination of several simple designs such as the Y-junction and the cross-channel for more complicated reactions. Adapted with the permission of Taylor & Francis.[54]

and high level of controllability. One silica glass capillary tube or stainless-steel tube can be utilized to fabricate continuous laminar flow microreactors. In this case, the reaction temperature in the microtube can be easily and accurately controlled with a water bath or an oil bath. Miscible solvents are pumped into the reactor, and their flow velocity or volume can be easily regulated by controlling the feed pump. Reagents are mixed by diffusion in laminar flow streams and microstructures like T-junction.[55] Membrane dispersion[56] can be implemented to enhance the mixing efficiency. However, one challenge for continuous laminar flow reactors is the potential blockage and fouling because of the narrow passage. The Luo group designed a microfiltration membrane dispersion microreactor to realize ultrafast and homogeneous mixing, thus minimizing blockage.[56,57]

Two immiscible flows (liquid–liquid system or gas–liquid system) are often used in segmented flow microreactors. The addition of a new phase triggers the recirculation movement, making the solution stretched and folded, and eventually improving the fluid mixing efficiency. On the other hand, continuous flows are cut into single columns in a segmented flow reactor. Each single column is a discrete encapsulated volume typically on the fL–nL scale and can be regarded as an independent microreactor. Thus, the back-mixing of the axial fluid in the single-phase flow microreactor is eliminated and the residence time can be accurately controlled.[58] This could help maintain a constant composition of reagents in all the reaction units. In addition, intensive segment-interval convective mixing could be induced at the cross of different flows, resulting in fast

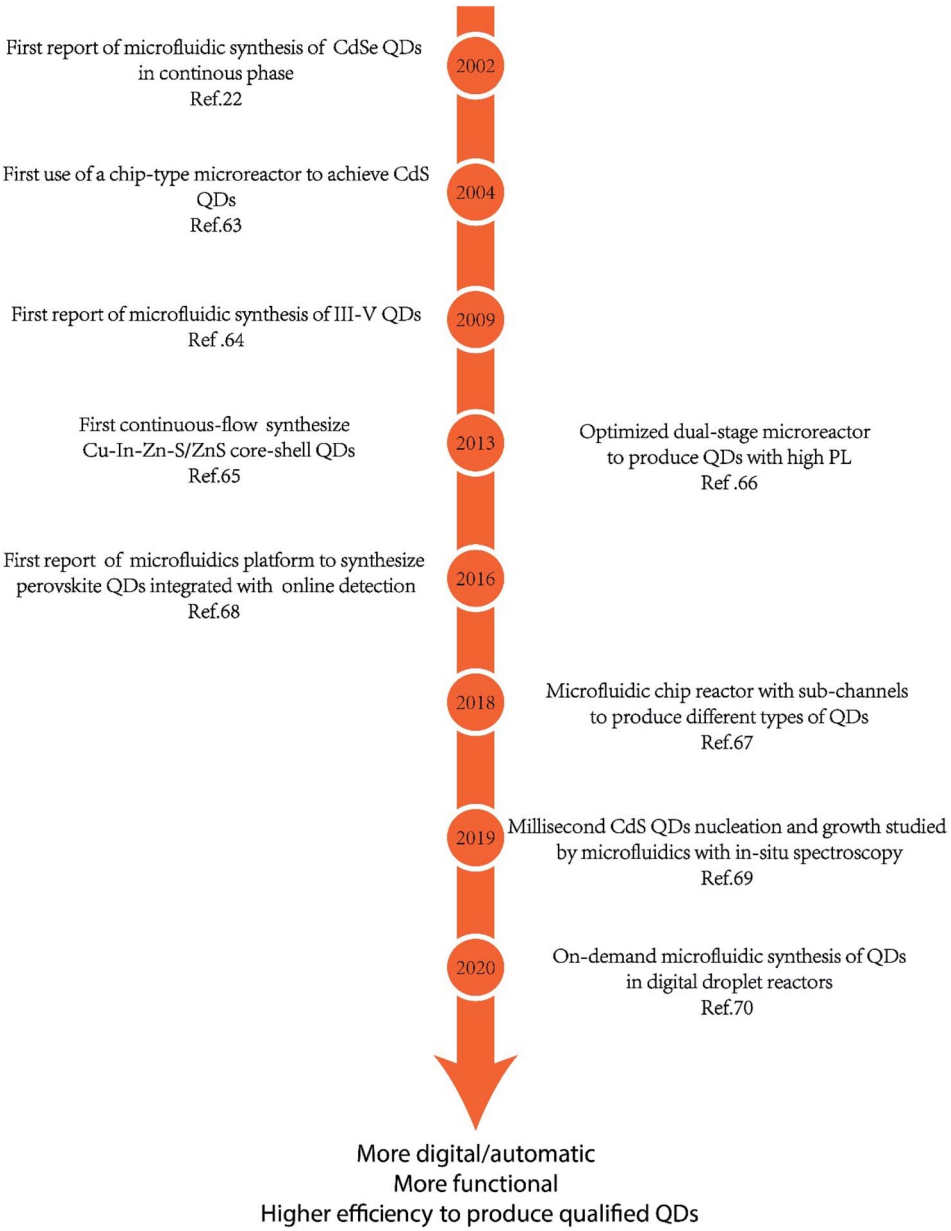

Fig. 3 Development timeline of microfluidic synthesis of QDs.

initiation of nucleation and shortening the time interval of nucleation.

Droplet-based microreactors are another type of multiphase flow reactors, generally including several liquid phase flows of reagents and another immiscible liquid phase flow as the carrier liquid for the generation of droplets. Similar to segmented flow microreactors, liquids are divided into independent parts, and back-mixing is eliminated. The difference is that the reaction mixture is not completely attached onto the channel walls. As a result, all products are mostly encapsulated within the confinement of individual droplets, finally minimizing the risk of clogging and fouling. Some typical designs for droplet generation include T-junction, Y-junction, cross-channel flow-focusing, and a combination of these basal geometries for more complicated reactions.[55] Another advantage is that droplet microfluidics shows great convenience in producing and manipulating droplets by operating immiscible flows inside microchannels.[59] By using microfluidic devices with different structures and modulating different hydrodynamic profiles such as flow phases and flowrates, single or multiple emulsions are generated to synthesize various QDs or encapsulate QDs inside microcapsules for further applications.

2.3 Microfluidic synthesis of quantum dots

Fig. 3 shows the general development of the microfluidic synthesis of QDs. Synthesis of CdX QDs has been extensively studied in the last few years. In 2002, Nakamura *et al.*[60] rejected the batch method of generating CdSe QDs and first synthesized CdSe QDs by using a continuous phase microfluidic device. In this research, different luminescence colors of CdSe were controlled by modulating the flow ratio of precursors and reaction temperature within the microfluidic device. In 2004, Shestopalov *et al.*[61] first discussed the use of a chip-type microreactor to achieve the synthesis of CdS QDs. The microfluidic synthesis of III–V QDs was first reported by Nightingale and de Mello[62] in 2009. The continuous-flow synthesis of Cu–In–Zn–S QDs inside microfluidic devices was first reported[63] in 2013. Microfluidic synthesis is not a simple alternative to flask reaction. Researchers could carefully design the reaction process and achieve more high-quality QDs with a more complex structure. Naughton *et al.*[64] developed a one-step procedure for liquid phase hot-injection synthesis of CdSe, CdS, and CdSeS (alloy) QDs. Remarkably, an additional module could produce QDs with complex structures, such as core–shell multi-layer CdSe@CdS@ZnS QDs. The complex core–shell multi-layer QDs showed a higher quantum yield (60%) compared to CdSe@ZnS QDs. An optimized dual-stage microreactor was reported to produce QDs with high PL[65] by precisely controlling the whole synthesis process, where nucleation and growth processes were separated in modules of different temperatures. Compared to QDs produced from conventional single-stage flow-synthesis, these QDs exhibited a high photoluminescence quantum yield (50%) and a narrow full width-half-maximum. Different designs of microfluidics offer opportunities to realize more functions in one production system. Micro-channels can be combined into chips to achieve more processes in one system. As shown in Fig. 4, Baek *et al.*[66] employed a microfluidic chip reactor with sub-channels to produce different types of QDs, including InP/ZnS, InP/ZnSe, InP/CdS, and InAs/InP. In this case, custom-designed chip reactors enabled precise control of heating profiles and flow distribution in the microchannels during the multistep reactions. In recent years, researchers have combined microfluidic devices with digital ligands to realize *in situ* detection and more automatic progress. In 2016, Lignos *et al.*[67] first reported a microfluidic platform to synthesize perovskite QDs integrated with the online detection for absorbance and fluorescence properties. The combination of online photoluminescence and absorption measurements as well as the fast mixing of reagents within such a platform allows the rigorous and rapid mapping of the reaction parameters, including molar ratios of Cs, Pb, and halide precursors, reaction temperatures, and reaction times. Seibt *et al.*[68] developed a microfluidic device where nucleation and growth of CdS QDs can be followed using *in situ* digital detectors on the time scale of the first 1–100 ms. This

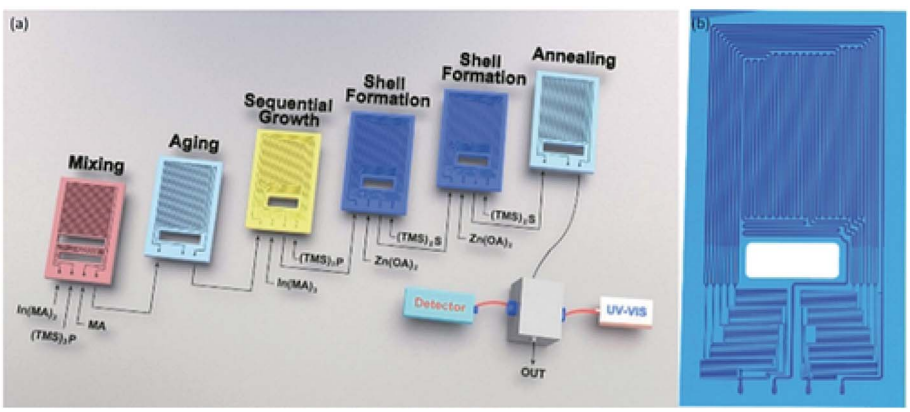

Fig. 4 (a) Multistage microfluidic platform for the synthesis of InP/ZnS core/shell QDs. The first three-stages (mixing, aging and sequential growth reactors) are used for the synthesis of InP cores and the following three-stages (two shell formation reactors and one annealing reactor) for the synthesis of core/shell morphologies. (b) The design of the shell-formation microreactor consisting of ten sub-channels. Reproduced with the permission of John Wiley & Sons.[66]

study provided direct and unique insights into early colloidal crystal nucleation and growth processes. In 2020, Richard *et al.*[69] utilized a liquid–liquid barrier between two immiscible liquids to generate a digital droplet reactor. In this case, a digitally regulated microfluidic device could ensure the delivery of precise amounts of reagents and the development of droplets.

Other microchannel structures have been used for more in-depth research or wider applications of QDs. Abolhasani *et al.*[70,71] reported the usage of oscillatory segmented flow (Fig. 5) as a compact microfluidic device that accommodates slow chemical reactions for the solution-phase processing of colloidal nanomaterials. In oscillatory segmented flow, a train of alternating gas bubbles and liquid reaction compartments (segmented flow) was initially formed, stopped and then subjected to a consistent back-and-forth motion. Compared to the continuous segmented flow, the oscillatory segmented flow significantly reduced the device space and removed the residence time limitation associated with continuous flow-based strategies. Hu *et al.*[72] employed a microfluidic chip setup to produce protein-functionalized CdTe QDs. Compared to functionalized QDs synthesized by the conventional bench-top method, the microfluidic-generated QDs have significantly higher protein-functionalization efficiency, photostability and colloidal stability.

Microfluidic approaches to CDs generally improve the synthesis efficiency, increase the quantum yields and have the potential to realize large-scale production. Rao *et al.*[73] developed a rapid, continuous CD synthesis technique by using a microreactor. The CDs could be synthesized at a large scale in less than 5 min, and a high quantum yield of 60.1% was achieved. Berenguel-Alonso *et al.*[74] reported the development of a fully integrated Low Temperature Co-Fired Ceramic (LTCC) microreactor for the synthesis of CDs. The microreactor integrates microfluidics, a heating resistor and an optical window for fluorescence imaging of the reaction progress in a monolithic and ceramic device. The obtained CDs exhibited blue photoluminescence with quantum yields up to 77%. As shown in Fig. 6, a microreactor with foamy copper[75] was also reported for the rapid synthesis of highly photoluminescent CDs. The quantum yield increased to 84.1%, which was two times higher compared to the procedure without adding foamy copper. In addition, different porosities of the applied foamy copper could influence the surface functional groups and the elemental content that directly affect the PL emission.

Perovskite QDs have outstanding optical properties, but have many limitations, such as poor thermal stability, photostability, water resistance, and anion exchange, and still require further investigations. Microfluidics cannot solve these problems from their roots but instead provide a desirable platform to study and optimize the characteristics of perovskite QDs. Reaction parameters in microfluidics can be easily and accurately controlled. Heating or mixture time can be reduced to seconds, thus minimizing side reactions before reaching the required reaction conditions. In addition, certain structures of perovskite QDs are so unstable that it is often impossible to collect accurate data of the reaction and/or of the product. Microfluidic devices anchored to *in situ* sensors have solved this problem in a great measure. The DeMello group[67] reported a droplet-based microfluidics platform to optimize the synthesis parameters for $CsPbX_3$ QDs. Online photoluminescence and absorption measurements were combined for rigorous and rapid mapping of the reaction parameters, including molar ratios of Cs, Pb, and halide precursors, reaction temperatures, and reaction

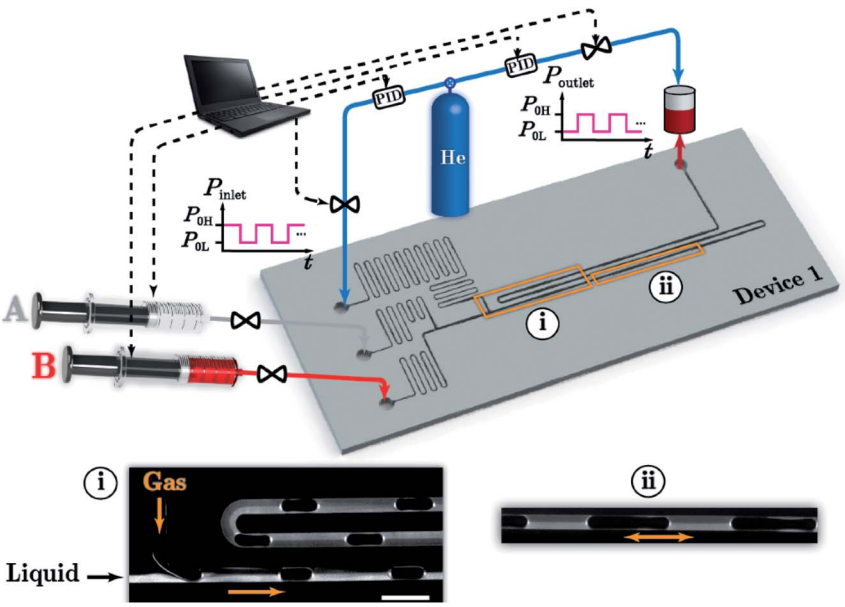

Fig. 5 Schematic illustration of the oscillatory segmented flow reaction system including device 1, four digital pressure regulators with built-in PID controllers, two syringe pumps, and a pressurized reservoir at the outlet. Inset (i) shows a typical fluorescence micrograph of a continuous gas–liquid segmented flow with two miscible liquid streams: clear (A) and fluorescence labelled (B) mineral oil. Inset (ii) shows the oscillatory segmented flow location. Reproduced with the permission of the Royal Society of Chemistry.[70]

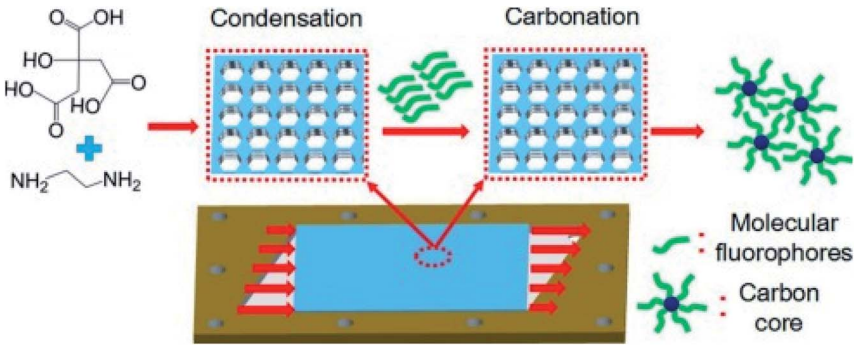

Fig. 6 The formation mechanism of N-CQDs synthesized using a microreactor with foamy copper having 98% porosity. Reproduced with the permission of Elsevier.[75]

times. Bao *et al.*[76] reported a simple, rapid, and stable method for the continuous synthesis of highly stable Cs_4PbBr_6 perovskite QDs using a microfluidic system. Relying on the easy controllability of the micro-channel, researchers tested different flow rates, reagent ratios, and crystal growth temperatures to optimize the Cs_4PbBr_6 perovskite production. Abdel-Latif *et al.*[77] developed a modular microfluidic platform, quantum dot exchanger, providing a comprehensive understanding of the halide exchange reactions in perovskite QDs. This research illustrated the effects of ligand composition and halide salt source on the rate and extent of the halide exchange reactions. Lignos *et al.*[78] fabricated a high-throughput automated microfluidic platform to study the synthesis of QDs of higher compositional complexity, *i.e.* $Cs_xFA_{1-x}Pb(Br_{1-y}I_y)_3$. In this case, researchers demonstrated the formation of QDs and successfully repeated the reaction in conventional reaction flasks with the parameters in microfluidics.

3 Applications in bio-sensing and bio-imaging

In comparison with organic dyes and fluorescent proteins, QDs have wide absorption, narrow emission, great chemical stability and resistance to photobleaching. These advantages make QDs suitable for fluorescence sensing and imaging. Developments in decreasing the toxicity and increasing the biocompatibility of QDs, as well as advances in surface engineering widen the applicability of QDs, especially in the field of biology. Studies on applications of QDs in bio-detection are mostly based on QDs from conventional methods, but recent achievements proved that QDs synthesized from microfluidics could be competent to conventional QDs and even behave better.

3.1 Applications in bio-sensing

Functionalized QDs were employed to test the concentration and distribution of biomarkers, such as macromolecules, small molecules and ions, within an organism. These data can indeed reflect the physiological status of the tested subject. The fluorescence status of functionalized QDs closely varies with the concentration of these biomarkers. According to the variation of fluorescence strength or emission wavelength of QDs, researchers could easily obtain the distribution of biomarkers in organisms. In addition, the abundant active groups on QDs give them the potential to combine with other molecules with high selectivity and give out more stable and accurate information.

Both the pH profile and metal cation gradients are crucial for maintaining cellular homeostasis and normal physiology. Liu *et al.*[79] synthesized mercaptoacetic acid (MAA)-capped CdSe/ZnSe/ZnS semiconductor QDs and utilized them as a pH sensor in living SKOV-3 human ovarian cancer cells. The luminescence intensity was enhanced 10 fold when the intracellular pH increased from 4 to 10. Xu *et al.*[80] gave explanations for the pH-sensitive photoluminescence of thiol-capped CdTe QDs. In the case of thiol-capped CdTe QDs, as the negatively charged form of the terminal group (COO^-) is converted to the uncharged form (COOH) when decreasing the pH from the original value (about 10) to the pK_a of the carboxylic group (about 4), the electrostatic repulsion between QDs is reduced, and more free ligands can easily diffuse into the QDs, leading to the improved ligand modification and enhanced PL of QDs. In this process, either removing surface trap sites or forming a thick shell leads to better surface passivation, resulting in stronger fluorescence signals. pH-sensitive QDs are employed to monitor reactions that involve pH variation or detect viruses that induce pH change to the medium.[81,82] CdTe QDs have been widely utilized for detecting heavy metal ions, and their selectivity and sensitivity can be tuned by utilizing different capping agents.[83] For example, thioglycolic acid (TGA)-capped CdTe QDs were utilized to detect Hg^{2+} in the nanomolar range, from 1.25×10^{-9} M to 1×10^{-8} M, with an LOD of 3.5×10^{-10} M Hg^{2+}. Besides, sulfur-doped CDs have been widely employed for the detection of Fe^{3+} ions.[84] In this research, a significant fluorescence quenching effect was observed with the addition of 200 μM Fe^{3+} while influence from other ions, including Zn^{2+}, Ni^{2+}, K^+, Mn^{2+}, Mg^{2+}, Cd^{2+}, Ca^{2+}, Cu^{2+}, and Ba^{2+}, was negligible. Our group[85] reported a facile and efficient microfluidic method to produce CDs with full-spectrum emission fluorescence. These CDs were used for Fe^{3+} detection and achieved the limit of detection at 4 μM.

Nucleic acid is one of the key biomarkers for the diagnosis of many diseases like cancers. Because of their high sensitivity and ability to detect small molecules, QDs have caught great

attention in the detection of nucleic acid, especially in complicated environments, *i.e.*, in the presence of many noise molecules or under harsh testing conditions. Han *et al.*[86] embedded QDs of different emissions into polymeric microbeads and realized multicolor optical coding. Polymeric microbeads functionalized with different oligonucleotide probes and conjugated with different QDs could emit distinguishable fluorescence signals at the attachment with different DNA sequences. As shown in Fig. 7, Zhang *et al.*[87] developed a rapid, highly sensitive, and specific miRNA assay based on the two-stage exponential amplification reaction (EXPAR) and a single-QD based nanosensor. Different miRNAs were converted to the same reporter oligonucleotides, which are later hybridized with the same set of capture and reporter probes to form sandwich hybrids. The resulting complexes consisting of fluorescence QDs, reporter oligonucleotides, and reporter probe Cy5, can discriminate single-nucleotide differences between miRNA family members with an optimized detection limit of 0.1 aM. Furthermore, Giri *et al.*[4] utilized QD barcode technology to detect genetic biomarkers of the bloodborne pathogens HIV, malaria, hepatitis B and C, and syphilis. In this case, QDs were barcoded to quickly detect nine different gene fragments stemming from five different infectious pathogens in a single sample volume. Recently, Nguyen *et al.*[88] reported a droplet microfluidic approach allowing high-quality QD–DNA conjugates to be produced using one single device. The subsequent experiments demonstrated that fluorescence response increased in the presence of 50–200 pmol of target strands. This study indicates the feasibility of using the droplet microfluidic platform for particle coating and other biochemical assays.

Proteins play an important role in physiological processes. Both their concentration and activity are crucial for biological processes. CdTe QDs were used as fluorescent probes to monitor changes in the working environment of enzymes. Xu *et al.*[89] reported a simple and novel method to profile protein kinase activity, avoiding tedious labeling or recognition treatment procedures. In this research, charge switching of peptide substrates was induced by kinase-catalyzed phosphorylation to mediate the aggregation of unmodified QDs, eventually resulting in an enhanced fluorescence and emission color change of QDs as a read-out. More general approaches for the protein analysis using QDs are based on QD surface engineering to recognize targeting molecules. Aqueous-phase-synthesized CdTe/CdS QDs were conjugated with secondary antibodies (goat anti-mouse IgG) to realize a versatile fluorescent probe for α-fetoprotein (AFP), *i.e.*, a common cancer biomarker.[5] In this

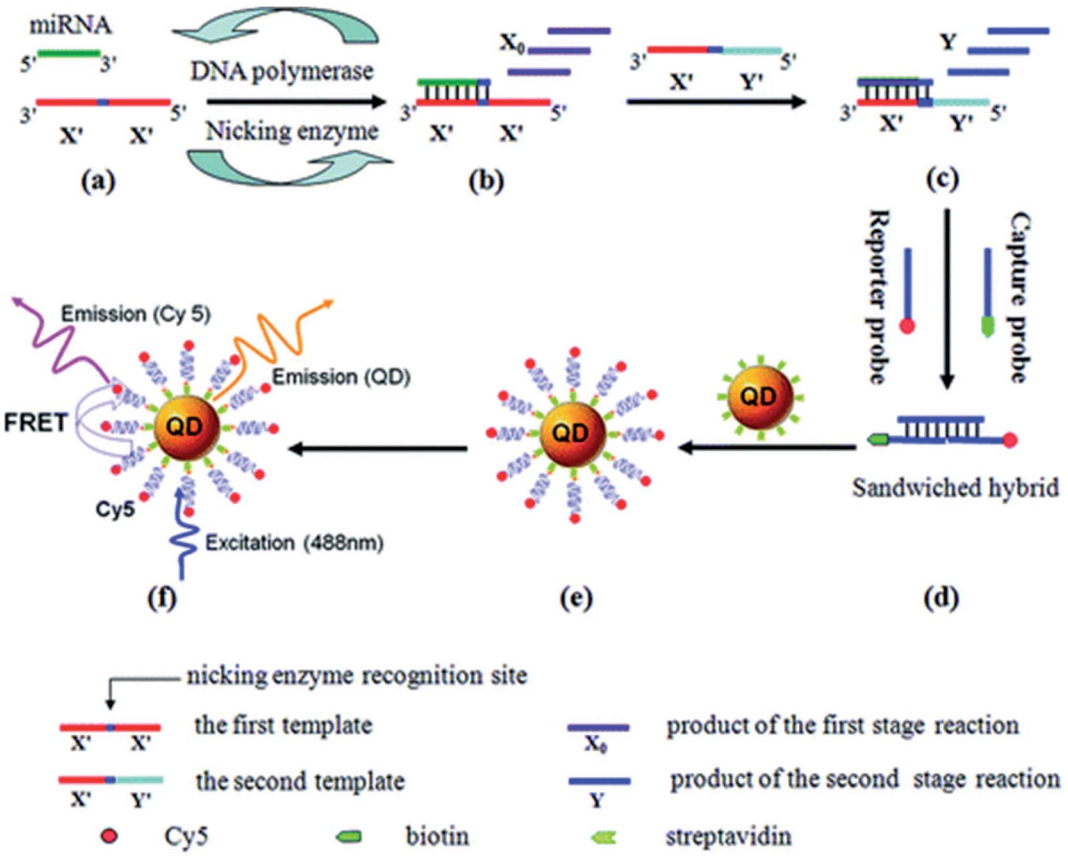

Fig. 7 (a) and (b) Exponential amplification of miRNA through the first-stage EXPAR reaction, (c) conversion of miRNA to the reporter oligonucleotide Y through the second-stage EXPAR reaction, (d) hybridization of the reporter oligonucleotide Y with two probes, (e) formation of the QD/reporter oligonucleotide Y/Cy5 complex through streptavidin–biotin binding, (f) fluorescence emission from Cy5 as a result of FRET between QDs and Cy5 at an excitation wavelength of 488 nm. Reproduced with the permission from ref. 87. Copyright (2012) American Chemical Society.

case, detection limits of cancer biomarkers were improved up to 250 fM, which represents an improvement in test sensitivity up to 4 orders of magnitude as compared to organic dyes. Advantages of high sensitivity were also shown in the detection of other proteins like biomarkers for Alzheimer's disease[90] or the intracellular cytoplasmic protein β-actin.[91] Ricardo *et al.*[92] reported a microfluidic method allowing control of the coupling between QDs and proteins. This microfluidic method improved the labelling process, and provided a rapid and efficient method that enabled the traceability of lectins. Furthermore, besides isolated protein molecules, QDs have been utilized in the detection of specific proteins on the surface of bacteria or cells when combining with magnetic materials, which can further improve the reliability and convenience of these methods.[93]

Conjugating dyes on the surface of QDs could result in Förster resonance energy transfer (FRET) and/or electron transfer processes, which increases the optical sensitivity and chemical stability of the produced QDs. Fig. 8 (ref. 94) illustrates the general mechanism of FRET. Conjugates offer the distinctive ability to produce discrete readouts, and serve as photoactivatable or photoswitchable probes to realize more functions. Ingram *et al.*[95] reported a ratiometric O_2 sensor based on QD conjugates. QDs were conjugated with an oxygen-quenching platinum(II)-octaethylporphyrin ketone (PtOEPK) to form FRET pairs, where emission of QDs provided perfect spectral overlap at the absorption peak of PtOEPK, allowing optimized FRET excitation. QD–PtOEPK conjugates were embedded into a polyvinyl chloride matrix to reduce the toxicity of QDs and enhance their sensitivity for O_2 concentration in biological microdomains of rat hippocampal brain tissue under seizure. Algar *et al.*[96] reported biomolecular assemblies of Tb^{3+} complex (Tb)-to-QD-to-Alexa Fluor 647 (A647) fluorescent dye multistep FRET relays, achieving multiplexed biosensing based on septotemporal resolution of QD-FRET without requiring multiple colors of QDs.

Besides fluorescence, the great electrochemical properties of QDs demonstrate their potential as electroactive species to release electrochemical signals. Liu *et al.*[97] reported a dual-channel detection of cancer cells with fluorescence and electrochemical signals. QDs were covalently assembled with DNA to form aptamer-DNA concatemer-QDs and later utilized to detect cancer cells using a @AuNP modified electrode. This cytosensor could distinguish cancer cells from normal cells and showed high sensitivity with the detection limit of 50 cells per mL. Du *et al.*[98] reported an electrochemical biosensor based on QDs that could specifically detect the change of E-cadherin, a member of the cadherin family, and analyze different stages of epithelial-mesenchymal transition (EMT). QDs were conjugated with E-cadherin antibody to serve as dual optical/electrochemical labels when carbon nanotubes–gold nanoparticles (CNTs–AuNPs) were used as the electrode. In addition, this biosensor can examine cells at different EMT stages and distinguish circulating tumor cells from tumor tissue cells *in situ*.

3.2 Applications in bio-imaging

Quantum dots have been widely used for cell labeling and other *in vitro* studies due to their excellent fluorescence properties. Since the concept of cell labeling based on QDs has already been proved,[99] design for more accurate and efficient labeling of designated cells or organelles has attracted more interest, especially for the efficient detection of specific tumor sites at both cellular and subcellular levels. Leevy *et al.*[100] reported extremely bright fluorescent imaging probes by treating the biotinylated zinc(II) dipicolylamine (Zn–DPA) probe with streptavidin-coated QDs. These probes could exhibit enhanced bacterial cell surface recognition properties and distinguish different mutants of the same bacterial species. Epidermal growth factor receptor (EGFR) is over-expressed in tumor cells and QDs conjugated to *anti*-EGFR antibodies could be used in

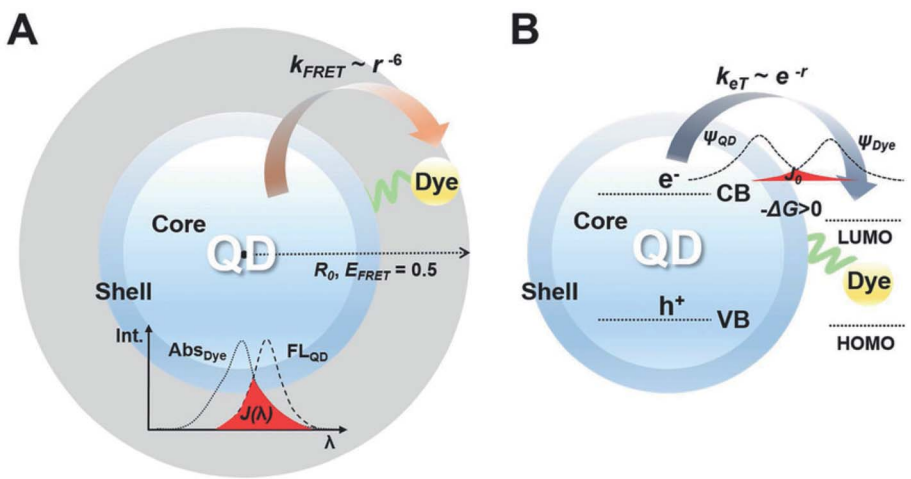

Fig. 8 (A) A FRET construct which consists of QDs and dye. Förster distance (R_0) determined from the center of QDs, indicating how FRET is effective. (B) An energy transfer construct that consists of QDs and dyes. The dye has the lowest unoccupied molecular orbital (LUMO) level between the band-edge states of the QDs, inducing a positive value of driving force ($-\Delta G > 0$). The electron orbital of the dye overlaps with the electron orbital of the QD, denoted as a red-colored area. Reproduced with the permission of John Wiley & Sons.[94]

conjunction with optical technologies to visualize the molecular changes involved during the development of cervical cancer.[101,102] Soleymani and his co-workers[103] synthesized folate decorated nitrogen-doped graphene QDs for the selective and specific detection of folate receptor-positive cancer cells. In this research, the resultant folic acid (FA)-decorated GQDs showed low photobleachability and cytotoxicity, and were stable for at least 2 months at 4 °C. Li *et al.*[104] utilized a microfluidic chip to produce aggregation-induced emission (AIE) QDs. Researchers achieved AIE QDs with NIR-II fluorescence and demonstrated that AIE QDs could enhance the tumor targeting and evasion from the liver more efficiently than conventional AIE dots.

While QDs are used as fluorescence probes for *in vivo* bioimaging, emission of far-red and near-infrared light in the spectral range 650–900 nm is preferred because they are isolated with the major absorption peaks of blood and water.[105] Gao *et al.*[106] prepared ultra-small near-infrared mercaptopropionic acid-coated InAs/InP/ZnSe QDs and successfully applied these QDs for *in vivo* imaging. Notably, due to the leaky tumor vasculatures, QDs pass through the normal blood vessels, then extravasate from the vessels when they reach the angiogenic tumor vessels, and finally accumulate preferentially at the tumor sites through the enhanced permeability and retention (EPR) effect. Transition metal ions are doped into QDs to obtain a larger Stokes shift, avoiding self-absorption/energy transfer, prolonging the excited-state lifetimes and improving QD stability. Sun *et al.*[107] prepared water-soluble Cu^{+} doped CdS QDs using a one-step synthesis method in a N_2 atmosphere. The resulting QDs possessed an ultra-small size (~5 nm), a high QY (25.6%), NIR emission (~700 nm) and low cytotoxicity, which allows them to serve as fluorescence probes to label living 3T3 cells. Avoiding the use of cadmium, Wu *et al.*[6] synthesized InP QDs applied for three-dimensional NIR visualization and combined QDs with an miRNA inhibitor in order to induce cancer cell apoptosis. As shown in Fig. 9, InP QDs were modified with the antibodies of vascular endothelial growth factor receptor 2 (VEGFR2), a characteristic molecule of tumor angiogenesis, to target leukemia K562 cells that highly expressed the latter biomarker. In addition, an oncogenic miRNA inhibitor was added to form an InP nanocomposite targeting K562 cells and induce apoptosis. Ding *et al.*[108] reported a method utilizing renewable and low-cost natural resources to synthesize highly efficient near-infrared emitting CDs. Pulp-free lemon juice was heated to synthesize NIR-CDs exhibiting excitation-independent photoluminescence emission at 704 nm. Hu *et al.*[109] demonstrated a fully automated method for preparing denatured bovine serum albumin (dBSA)–$CuInS_2$/ZnS QDs by introducing microfluidic chips in the synthesis of biofunctionalized QDs. The emission wavelength of the dBSA–$CuInS_2$/ZnS QDs is located in the near-infrared range and can be tuned from 650 to 750 nm. The cell images showed that biomolecule-modified QDs yielded good results for HepG-2 and Panc-1 cells.

Multimodal imaging has been shown to be advantageous to utilize complementary information of each imaging mode, and combine different modes in a single material system for synergetic imaging. Magnetic resonance imaging (MRI) has been developed for clinical applications and an MRI contrast agent was conjugated with QDs to form imaging probes with multimodalities. Yong[110] prepared Mn-doped CdTeSe/CdS QDs with near-infrared emission by a one-pot synthesis approach. These Mn-doped QDs, possessing excellent luminescence and paramagnetic properties, were conjugated with biomolecules to be selectively delivered to pancreatic cancer cells. As shown in Fig. 10, Pan *et al.*[111] reported the facile synthesis of a type of carbon QDs based dual-modal fluorescence/magnetic resonance imaging probe by doping Gd(III) into carbon QDs. In this case, Gd^{3+} content was only 1.0% (w/w) in CDs, guaranteeing excellent biocompatibility and blood compatibility. Dual-modality bioimaging applications of GCDs were successfully demonstrated by the use of HeLa cells and mice as models. The experimental results showcased that the addition of GCDs significantly enhanced MR response when compared to commercially available contrast agents while still exhibiting strong fluorescence brightness with major improvement in QY. Liu *et al.*[112] synthesized superparamagnetic nitrogen-doped carbon iron oxide hybrid quantum dots (C–Fe_3O_4 QDs). The prepared C–Fe_3O_4 QDs exhibited wavelength-tunable fluorescence property with high quantum yield and strong superparamagnetic property. The *in vivo* bioimaging of tumor-

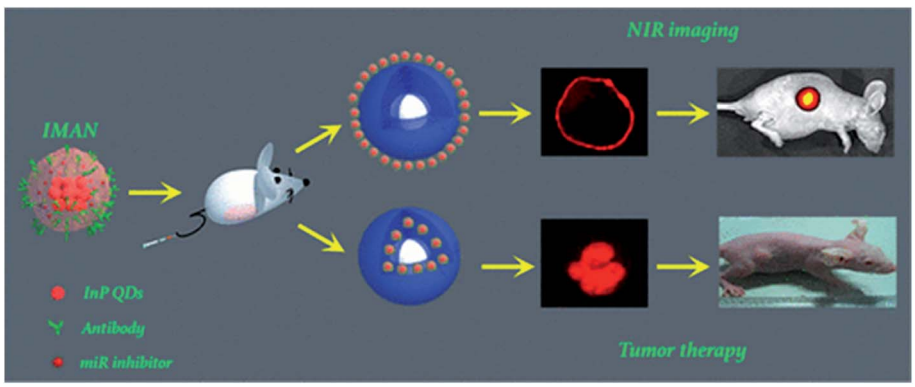

Fig. 9 An InP nanocomposite, which combines a VEGFR2 antibody and an miR92a inhibitor loaded on InP QDs, was developed as an NIR imaging target and drug delivery vector, which remarkably targeted human myelogenous leukemia cells *in vitro* and *in vivo*, inducing apoptosis and inhibiting tumor growth. Reproduced with the permission from ref. 6. Copyright (2017) American Cheimical Society.

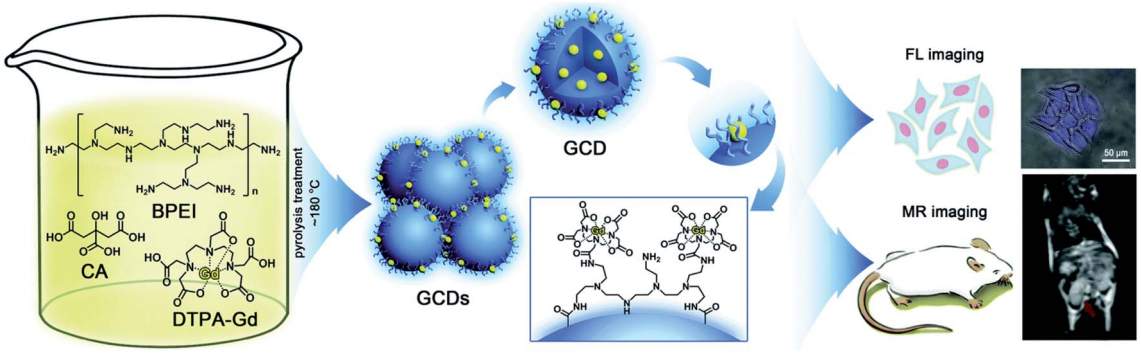

Fig. 10 Schematic illustration of the synthesis and dual-modality imaging application of GCDs. Reproduced with the permission of the Royal Society of Chemistry.[111]

bearing nude mice by combining FL, MR, and CT images further demonstrates that the as-prepared C–Fe_3O_4 QDs can be readily and efficiently used in FL/MR/CT triple-modal tumor imaging.

4 Conclusions and perspectives

Quantum dots, as an effective alternative to traditional dye materials, have been widely used in the field of bio-sensing and bio-imaging because of their excellent optical properties and biocompatibility. NIR QDs, targeting QDs and nontoxic QDs have been explored to adapt to the biological working environment and conform to the requirements of clinical applications. While properties of QDs highly depend on the precise control of reaction conditions, microfluidic devices provide a reliable and multifunctional platform to produce high-quality QDs through precise controlling of the reaction environment and expansibility with extra automation. The implementation of microfluidic technology greatly simplifies the fabrication of QDs with overall excellent controllability of the generation process, and offers new opportunities for its future industrialization. By tuning different reaction parameters in the microreactor, not only one can modulate and regulate the size and composition of the generated QDs, but also modify and/or even functionalize QDs with more complex features in order to meet the requirements of downstream applications.

Microreactors provide a uniform QD generation environment, which enables precise control over the reaction time, reactant ratio and reaction process by simply regulating flow rates. In addition, digital ligands are combined with microreactors to study and optimize the characteristics of QDs. We believe that more researchers in the quantum dot community will adopt microfluidics as the synthesis and analysis platform to further explore new technology and parametric landscapes. For the purpose of further simplifying the detection process and enhancing the system automation, coupling of microfluidics and related equipment will become an effective solution for the practical use of the process. With the development of low-cost and high reliability microfluidic devices, QDs are expected to be extended to clinical practices. However, microfluidic synthesis of QDs still faces some challenges and problems before its wide application in clinical practices even with the above advantages. On one hand, microfluidic synthesis of QDs is at a relatively early stage. Some key fatal problems such as clogging and relatively low throughput have not been perfectly solved. Due to the small dimensions of the operating microchannels and the increased pressure drop with increasing flow rate, the current maximum mass production rate is limited and is lower than that of conventional methods. On the other hand, the most widely carried out research on the applications of QDs is based on traditional batch or flask reaction and QDs from microfluidics do not demonstrate overall performance beyond those conventional methods. Microfluidic synthesis of QDs does not exhibit complete irreplaceability but we have seen that microfluidic synthesis methods contribute to a rapid synthesis and efficient functionalization of QDs. Furthermore, microfluidic synthesis of QDs can provide abundant data and information *in situ* to help researchers understand and modify the produced QDs. We expect more researchers from biology, chemistry, materials and other fields to unify the problems in application and promote the final clinical practice of QDs and even other nanomaterials.

Author contributions

Yu Cheng prepared the original draft and did the editing. Yundong Wang and Jianhong Xu contributed to the funding acquisition, methodology, supervision and reviewing of the manuscript. Yuhao Geng and Si Da Ling provided help in methodology and editing.

Conflicts of interest

There are no conflicts to declare.

Acknowledgements

The authors gratefully acknowledge the support of the National Natural Science Foundation of China (22025801, 21991100, 21991101).

References

1 X. Michalet, F. F. Pinaud, L. A. Bentolila, J. M. Tsay, S. Doose, J. J. Li, G. Sundaresan, A. M. Wu, S. S. Gambhir and S. Weiss, *Science*, 2005, **307**, 538–544.
2 Y. Park, S. Jeong and S. Kim, *J. Photochem. Photobiol., C*, 2017, **30**, 51–70.
3 S. Chinnathambi, S. Chen, S. Ganesan and N. Hanagata, *Adv. Healthcare Mater.*, 2014, **3**, 10–29.
4 S. Giri, E. A. Sykes, T. L. Jennings and W. C. W. Chan, *ACS Nano*, 2011, **5**, 1580–1587.
5 M. Hu, J. Yan, Y. He, H. T. Lu, L. X. Weng, S. P. Song, C. H. Fan and L. H. Wang, *ACS Nano*, 2010, **4**, 488–494.
6 Y. Z. Wu, J. Sun, Y. Q. Zhang, M. M. Pu, G. Zhang, N. Y. He and X. Zeng, *ACS Appl. Mater. Interfaces*, 2017, **9**, 13068–13078.
7 J. Sui, J. Yan, D. Liu, K. Wang and G. Luo, *Small*, 2020, **16**, e1902828.
8 J. P. McMullen and K. F. Jensen, *Org. Process Res. Dev.*, 2011, **15**, 398–407.
9 I. Lignos, R. Maceiczyk and A. J. deMello, *Acc. Chem. Res.*, 2017, **50**, 1248–1257.
10 A. Schiener, A. Magerl, A. Krach, S. Seifert, H. G. Steinruck, J. Zagorac, D. Zahn and R. Weihrich, *Nanoscale*, 2015, **7**, 11328–11333.
11 R. Rossetti, S. Nakahara and L. E. Brus, *J. Chem. Phys.*, 1983, **79**, 1086–1088.
12 D. J. N. C. B. Murray and M. G. Bawendi, *J. Am. Chem. Soc.*, 1993, **115**(19), 8706–8715.
13 W. W. Yu and X. G. Peng, *Angew. Chem., Int. Ed.*, 2002, **41**, 2368–2371.
14 Z. A. Peng and X. G. Peng, *J. Am. Chem. Soc.*, 2001, **123**, 183–184.
15 D. W. Bahnemann, C. Kormann and M. R. Hoffmann, *J. Phys. Chem.*, 1987, **91**, 3789–3798.
16 S. Mahamuni, A. A. Khosravi, M. Kundu, A. Kshirsagar, A. Bedekar, D. B. Avasare, P. Singh and S. K. Kulkarni, *J. Appl. Phys.*, 1993, **73**, 5237–5240.
17 M. C. H. Liao, Y. H. Change, C. C. Tsai, M. H. Chieng and Y. F. Chen, *J. Appl. Phys.*, 1999, **86**, 4694–4696.
18 B. O. Dabbousi, J. RodriguezViejo, F. V. Mikulec, J. R. Heine, H. Mattoussi, R. Ober, K. F. Jensen and M. G. Bawendi, *J. Phys. Chem. B*, 1997, **101**, 9463–9475.
19 A. A. Guzelian, J. E. B. Katari, A. V. Kadavanich, U. Banin, K. Hamad, E. Juban, A. P. Alivisatos, R. H. Wolters, C. C. Arnold and J. R. Heath, *J. Phys. Chem.*, 1996, **100**, 7212–7219.
20 J. Lim, W. K. Bae, D. Lee, M. K. Nam, J. Jung, C. Lee, K. Char and S. Lee, *Chem. Mater.*, 2011, **23**, 4459–4463.
21 A. A. Guzelian, U. Banin, A. V. Kadavanich, X. Peng and A. P. Alivisatos, *Appl. Phys. Lett.*, 1996, **69**, 1432–1434.
22 E. Werwa, A. A. Seraphin, L. A. Chiu, C. X. Zhou and K. D. Kolenbrander, *Appl. Phys. Lett.*, 1994, **64**, 1821–1823.
23 Z. H. Kang, Y. Liu, C. H. A. Tsang, D. D. D. Ma, X. Fan, N. B. Wong and S. T. Lee, *Adv. Mater.*, 2009, **21**, 661–664.
24 K. Fujioka, M. Hiruoka, K. Sato, N. Manabe, R. Miyasaka, S. Hanada, A. Hoshino, R. D. Tilley, Y. Manome, K. Hirakuri and K. Yamamoto, *Nanotechnology*, 2008, **19**, 415102.
25 J. H. Park, L. Gu, G. von Maltzahn, E. Ruoslahti, S. N. Bhatia and M. J. Sailor, *Nat. Mater.*, 2009, **8**, 331–336.
26 B. Ghosh and N. Shirahata, *Sci. Technol. Adv. Mater.*, 2014, **15**, 014207.
27 P. M. Allen and M. G. Bawendi, *J. Am. Chem. Soc.*, 2008, **130**, 9240–9241.
28 L. Li, T. J. Daou, I. Texier, T. K. C. Tran, Q. L. Nguyen and P. Reiss, *Chem. Mater.*, 2009, **21**, 2422–2429.
29 X. Y. Xu, R. Ray, Y. L. Gu, H. J. Ploehn, L. Gearheart, K. Raker and W. A. Scrivens, *J. Am. Chem. Soc.*, 2004, **126**, 12736–12737.
30 M. Nurunnabi, Z. Khatun, K. M. Huh, S. Y. Park, D. Y. Lee, K. J. Cho and Y. K. Lee, *ACS Nano*, 2013, **7**, 6858–6867.
31 S. Sagbas and N. Sahiner, *Nanocarbon and Its Composites: Preparation, Properties, and Applications*, 2019, pp. 651–676, DOI: 10.1016/b978-0-08-102509-3.00022-5.
32 H. Ali, S. Ghosh and N. Jana, *Wiley Interdiscip. Rev.: Nanomed. Nanobiotechnol.*, 2020, **12**, e1617.
33 Z. Kang and S. Lee, *Nanoscale*, 2019, **11**, 19214–19224.
34 L. Xiao and H. D. Sun, *Nanoscale Horiz.*, 2018, **3**, 565–597.
35 J. G. Zhou, C. Booker, R. Y. Li, X. T. Zhou, T. K. Sham, X. L. Sun and Z. F. Ding, *J. Am. Chem. Soc.*, 2007, **129**, 744–745.
36 J. Lu, J. X. Yang, J. Z. Wang, A. L. Lim, S. Wang and K. P. Loh, *ACS Nano*, 2009, **3**, 2367–2375.
37 A. B. Bourlinos, A. Stassinopoulos, D. Anglos, R. Zboril, V. Georgakilas and E. P. Giannelis, *Chem. Mater.*, 2008, **20**, 4539–4541.
38 H. Peng and J. Travas-Sejdic, *Chem. Mater.*, 2009, **21**, 5563–5565.
39 S. Zhu, Q. Meng, L. Wang, J. Zhang, Y. Song, H. Jin, K. Zhang, H. Sun, H. Wang and B. Yang, *Angew. Chem., Int. Ed.*, 2013, **52**, 3953–3957.
40 L. L. Zhang, Y. J. Han, J. B. Zhu, Y. L. Zhai and S. J. Dong, *Anal. Chem.*, 2015, **87**, 2033–2036.
41 Z. Wang, L. J. Cao, Y. M. Ding, R. Shi, X. J. Wang, H. Lu, Z. D. Liu, F. Xiu, J. Q. Liu and W. Huang, *RSC Adv.*, 2017, **7**, 21969–21973.
42 J. Z. Guo, H. Li, L. T. Ling, G. Li, R. Cheng, X. Lu, A. Q. Xie, Q. Li, C. F. Wang and S. Chen, *ACS Sustainable Chem. Eng.*, 2020, **8**, 1566–1572.
43 S. Chandra, A. R. Chowdhuri, T. K. Mahto, A. Samui and S. K. Sahu, *RSC Adv.*, 2016, **6**, 72471–72478.
44 D. Weber, *Z. Naturforsch., B: J. Chem. Sci.*, 1978, **33**, 1443–1445.
45 D. B. Mitzi, C. A. Feild, Z. Schlesinger and R. B. Laibowitz, *J. Solid State Chem.*, 1995, **114**, 159–163.
46 D. B. Mitzi, *Prog. Inorg. Chem.*, 1999, **48**, 1–121.
47 J. Lei, F. Gao, H. X. Wang, J. Li, J. X. Jiang, X. Wu, R. R. Gao, Z. Yang and S. Z. Liu, *Sol. Energy Mater. Sol. Cells*, 2018, **187**, 1–8.

48 L. Protesescu, S. Yakunin, M. I. Bodnarchuk, F. Krieg, R. Caputo, C. H. Hendon, R. X. Yang, A. Walsh and M. V. Kovalenko, *Nano Lett.*, 2015, **15**, 3692–3696.
49 X. M. Li, Y. Wu, S. L. Zhang, B. Cai, Y. Gu, J. Z. Song and H. B. Zeng, *Adv. Funct. Mater.*, 2016, **26**, 2435–2445.
50 T. C. Jellicoe, J. M. Richter, H. F. J. Glass, M. Tabachnyk, R. Brady, S. E. Dutton, A. Rao, R. H. Friend, D. Credgington, N. C. Greenham and M. L. Bohm, *J. Am. Chem. Soc.*, 2016, **138**, 2941–2944.
51 J. Zhang, Y. Yang, H. Deng, U. Farooq, X. K. Yang, J. Khan, J. Tang and H. S. Song, *ACS Nano*, 2017, **11**, 9294–9302.
52 Q. C. Zhou, Z. L. Bai, W. G. Lu, Y. T. Wang, B. S. Zou and H. Z. Zhong, *Adv. Mater.*, 2016, **28**, 9163–9168.
53 C. Y. Zhang, B. Wang, W. B. Li, S. Q. Huang, L. Kong, Z. C. Li and L. Li, *Nat. Commun.*, 2017, **8**, 1138.
54 N. Hao, Y. Nie and J. X. J. Zhang, *Int. Mater. Rev.*, 2018, **63**, 461–487.
55 S. I. Kawasaki, K. Sue, R. Ookawara, Y. Wakashima, A. Suzuki, Y. Hakuta and K. Arai, *J. Supercrit. Fluids*, 2010, **54**, 96–102.
56 G. G. Chen, G. S. Luo, J. H. Xu and J. D. Wang, *Powder Technol.*, 2004, **139**, 180–185.
57 G. G. Chen, G. S. Luo, X. R. Yang, Y. W. Sun and J. D. Wang, *Mater. Sci. Eng., A*, 2004, **380**, 320–325.
58 A. Gunther and K. F. Jensen, *Lab Chip*, 2007, **7**, 935.
59 L. R. Shang, Y. Cheng and Y. J. Zhao, *Chem. Rev.*, 2017, **117**, 7964–8040.
60 B. K. H. Yen, N. E. Stott, K. F. Jensen and M. G. Bawendi, *Adv. Mater.*, 2003, **15**, 1858–1862.
61 I. Shestopalov, J. D. Tice and R. F. Ismagilov, *Lab Chip*, 2004, **4**, 316–321.
62 A. M. Nightingale and J. C. de Mello, *ChemPhysChem*, 2009, **10**, 2612–2614.
63 S. J. Li, Y. Y. Chen, L. J. Huang and D. C. Pan, *Nanotechnology*, 2013, **24**, 395705.
64 M. S. Naughton, V. Kumar, Y. Bonita, K. Deshpande and P. J. A. Kenis, *Nanoscale*, 2015, **7**, 15895–15903.
65 J. Pan, A. O. El-Ballouli, L. Rollny, O. Voznyy, V. M. Burlakov, A. Goriely, E. H. Sargent and O. M. Bakr, *ACS Nano*, 2013, **7**, 10158–10166.
66 J. Baek, Y. Shen, I. Lignos, M. G. Bawendi and K. F. Jensen, *Angew. Chem., Int. Ed.*, 2018, **57**, 10915–10918.
67 I. Lignos, S. Stavrakis, G. Nedelcu, L. Protesescu, A. J. Demello and M. V. Kovalenko, *Nano Lett.*, 2016, **16**, 1869–1877.
68 S. Seibt, P. Mulvaney and S. Forster, *Colloids Surf., A*, 2019, **562**, 263–269.
69 C. Richard, R. McGee, A. Goenka, P. Mukherjee and R. Bhargava, *Ind. Eng. Chem. Res.*, 2020, **59**, 3730–3735.
70 M. Abolhasani, A. Oskooei, A. Klinkova, E. Kumacheva and A. Gunther, *Lab Chip*, 2014, **14**, 2309–2318.
71 M. Abolhasani, C. W. Coley, L. S. Xie, O. Chen, M. G. Bawendi and K. F. Jensen, *Chem. Mater.*, 2015, **27**, 6131–6138.
72 S. Y. Hu, S. W. Zeng, B. T. Zhang, C. B. Yang, P. Y. Song, T. J. H. Danny, G. M. Lin, Y. C. Wang, T. Anderson, P. Coquet, L. W. Liu, X. H. Zhang and K. T. Yong, *Analyst*, 2014, **139**, 4681–4690.
73 L. S. Rao, Y. Tang, Z. T. Li, X. R. Ding, G. W. Liang, H. G. Lu, C. M. Yan, K. R. Tang and B. H. Yu, *Mater. Sci. Eng., C*, 2017, **81**, 213–223.
74 M. Berenguel-Alonso, I. Ortiz-Gómez, B. Fernández, P. Couceiro, J. Alonso-Chamarro, L. F. Capitán-Vallvey, A. Salinas-Castillo and M. Puyol, *Sens. Actuators, B*, 2019, **296**, 126613.
75 Y. Tang, L. S. Rao, Z. T. Li, H. G. Lu, C. M. Yan, S. D. Yu, X. R. Ding and B. H. Yu, *Sens. Actuators, B*, 2018, **258**, 637–647.
76 Z. Bao, H. C. Wang, Z. F. Jiang, R. J. Chung and R. S. Liu, *Inorg. Chem.*, 2018, **57**, 13071–13074.
77 K. Abdel-Latif, R. W. Epps, C. B. Kerr, C. M. Papa, F. N. Castellano and M. Abolhasani, *Adv. Funct. Mater.*, 2019, **29**, 1900712.
78 I. Lignos, V. Morad, Y. Shynkarenko, C. Bernasconi, R. M. Maceiczyk, L. Protesescu, F. Bertolotti, S. Kumar, S. T. Ochsenbein, N. Masciocchi, A. Guagliardi, C. J. Shih, M. I. Bodnarchuk, A. J. deMello and M. V. Kovalenko, *ACS Nano*, 2018, **12**, 5504–5517.
79 Y. S. Liu, Y. H. Sun, P. T. Vernier, C. H. Liang, S. Y. C. Chong and M. A. Gundersen, *J. Phys. Chem. C*, 2007, **111**, 2872–2878.
80 S. Xu, C. Wang, H. Zhang, Z. Wang, B. Yang and Y. Cui, *Nanotechnology*, 2011, **22**, 315703.
81 D. H. Yu, Z. Wang, Y. Liu, L. Jin, Y. M. Cheng, J. G. Zhou and S. G. Cao, *Enzyme Microb. Technol.*, 2007, **41**, 127–132.
82 Z. T. Deng, Y. Zhang, J. C. Yue, F. Q. Tang and Q. Wei, *J. Phys. Chem. B*, 2007, **111**, 12024–12031.
83 M. Labeb, A. H. Sakr, M. Soliman, T. M. Abdel-Fettah and S. Ebrahim, *Opt. Mater.*, 2018, **79**, 331–335.
84 Q. Xu, P. Pu, J. G. Zhao, C. B. Dong, C. Gao, Y. S. Chen, J. R. Chen, Y. Liu and H. J. Zhou, *J. Mater. Chem. A*, 2015, **3**, 542–546.
85 M. Shao, Q. Yu, N. Jing, Y. Cheng, D. Wang, Y. D. Wang and J. H. Xu, *Lab Chip*, 2019, **19**, 3974–3978.
86 M. Y. Han, X. H. Gao, J. Z. Su and S. Nie, *Nat. Biotechnol.*, 2001, **19**, 631–635.
87 Y. Zhang and C. Y. Zhang, *Anal. Chem.*, 2012, **84**, 224–231.
88 T. H. Nguyen, A. Sedighi, U. J. Krull and C. L. Ren, *ACS Sens.*, 2020, **5**, 746–753.
89 X. H. Xu, X. Liu, Z. Nie, Y. L. Pan, M. L. Guo and S. Z. Yao, *Anal. Chem.*, 2011, **83**, 52–59.
90 E. Morales-Narvaez, H. Monton, A. Fomicheva and A. Merkoci, *Anal. Chem.*, 2012, **84**, 6821–6827.
91 S. Kale, A. Kale, H. Gholap, A. Rana, R. Desai, A. Banpurkar, S. Ogale and P. Shastry, *J. Nanopart. Res.*, 2012, **14**, 732.
92 R. Cervantes-Jimenez, L. Sanchez-Segura, L. E. Estrada-Martinez, A. Topete-Camacho, E. Mendiola-Olaya, A. N. Rosas-Escareno, C. Saldana-Gutierrez, M. E. Figueroa-Cabanas, J. L. Dena-Beltran, A. Kuri-Garcia, A. Blanco-Labra and T. Garcia-Gasca, *Molecules*, 2020, **25**, 1041.
93 H. Wang, Y. B. Li, A. Wang and M. Slavik, *J. Food Prot.*, 2011, **74**, 2039–2047.

94 S. Jung and X. Chen, *Adv. Healthcare Mater.*, 2018, **7**, e1800252.
95 J. M. Ingram, C. F. Zhang, J. Xu and S. J. Schiff, *J. Neurosci. Methods*, 2013, **214**, 45–51.
96 W. R. Algar, D. Wegner, A. L. Huston, J. B. Blanco-Canosa, M. H. Stewart, A. Armstrong, P. E. Dawson, N. Hildebrandt and I. L. Medintz, *J. Am. Chem. Soc.*, 2012, **134**, 1876–1891.
97 H. Y. Liu, S. M. Xu, Z. M. He, A. P. Deng and J. J. Zhu, *Anal. Chem.*, 2013, **85**, 3385–3392.
98 X. Du, Z. H. Zhang, X. D. Zheng, H. Y. Zhang, D. Dong, Z. G. Zhang, M. Liu and J. Zhou, *Nat. Commun.*, 2020, **11**, 192.
99 W. C. W. Chan and S. M. Nie, *Science*, 1998, **281**, 2016–2018.
100 W. M. Leevy, T. N. Lambert, J. R. Johnson, J. Morris and B. D. Smith, *Chem. Commun.*, 2008, 2331–2333, DOI: 10.1039/b803590c.
101 D. L. Nida, M. S. Rahman, K. D. Carlson, R. Richards-Kortum and M. Follen, *Gynecol. Oncol.*, 2005, **99**, S89–S94.
102 N. Kawashima, K. Nakayama, K. Itoh, T. Itoh, M. Ishikawa and V. Biju, *Chem.–Eur. J.*, 2010, **16**, 1186–1192.
103 J. Soleymani, M. Hasanzadeh, M. H. Somi, S. A. Ozkan and A. Jouyban, *Int. J. Biol. Macromol.*, 2018, **118**, 1021–1034.
104 X. Li, M. Zha, Y. Li, J.-S. Ni, T. Min, T. Kang, G. Yang, H. Tang, K. Li and X. Jiang, *Angew. Chem., Int. Ed.*, 2020, **59**, 21899–21903.
105 V. Ntziachristos, C. Bremer and R. Weissleder, *Eur. Radiol.*, 2003, **13**, 195–208.
106 J. H. Gao, K. Chen, R. G. Xie, J. Xie, S. Lee, Z. Cheng, X. G. Peng and X. Y. Chen, *Small*, 2010, **6**, 256–261.
107 T. T. Sun, M. Wu, X. W. He, W. Y. Li and X. Z. Feng, *J. Mater. Chem. B*, 2015, **3**, 6971–6978.
108 H. Ding, X. X. Zhou, B. T. Qin, Z. Y. Zhou and Y. P. Zhao, *J. Lumin.*, 2019, **211**, 298–304.
109 S. Y. Hu, B. T. Zhang, S. W. Zeng, L. W. Liu, K. T. Yong, H. B. Ma and Y. G. Tang, *Lab Chip*, 2020, **20**, 3001–3010.
110 K. T. Yong, *Nanotechnology*, 2009, **20**, 015102.
111 Y. Pan, J. Yang, Y. N. Fang, J. H. Zheng, R. Song and C. Q. Yi, *J. Mater. Chem. B*, 2017, **5**, 92–101.
112 X. L. Liu, H. Jiang, J. Ye, C. Q. Zhao, S. P. Gao, C. Y. Wu, C. H. Li, J. C. Li and X. M. Wang, *Adv. Funct. Mater.*, 2016, **26**, 8694–8706.